Dalton Transactions

PAPER

Cite this: *Dalton Trans.*, 2015, **44**, 11491

Synthesis, structure, and spectral and electrochemical properties of chromium(III) tris-(8-hydroxyquinolinate)†

Ana R. Freitas,[a] Mónica Silva,[a] M. Luísa Ramos,[a] Licínia L. G. Justino,[a] Sofia M. Fonseca,[a] Madalina M. Barsan,[b] Christopher M. A. Brett,[b] M. Ramos Silva[c] and Hugh D. Burrows*[a]

Received 18th February 2015, Accepted 7th May 2015

DOI: 10.1039/c5dt00727e

www.rsc.org/dalton

The kinetically inert chromium(III) tris-(8-hydroxyquinolinate), Crq_3, has been synthesized, crystallized from 90% methanol–water, and characterized by MALDI-TOF mass spectrometry, thermogravimetry, FTIR, NMR spectroscopy, and X-ray powder diffraction. It is formed as a methanol solvate, but the solvent can be removed by heating. Large paramagnetic shifts and spectral broadening in ^1H NMR spectra indicate electron delocalization between the metal and the ligand. DFT calculations show it is present as the meridional isomer, with the HOMO largely based on one of the metal 3d orbitals and the LUMO essentially localized on the ligands. Cyclic voltammetry (CV) in acetonitrile solutions shows four oxidation peaks and two, less intense reduction waves on the first scan. The HOMO energy determined from the first oxidation peak is fairly close to that obtained by DFT, in agreement with this being mainly metal based. Although the number of peaks decreases on subsequent CV scans, the complex shows markedly enhanced electrochemical stability compared with aluminium(III) tris-(8-hydroxyquinolinate). Solution UV/visible absorption and solid diffuse reflectance spectra have a weak, long wavelength band, assigned to the metal based d–d transition, in addition to the normal, ligand based bands seen in metal quinolates. The energy of the lowest energy band is identical to the HOMO–LUMO separation obtained by cyclic voltammetry, in agreement with the above description. The compound is only weakly luminescent, in contrast to many other metal quinolates, due to the lowest energy transition being metal rather than ligand based. The potential of this compound as an electron transporting/hole blocking layer in optoelectronic devices is indicated.

1. Introduction

Metal complexes of 8-hydroxyquinoline (sometimes termed oxinates) have been known for over a century.[1] Complexes of 8-hydroxyquinoline and its derivatives with metal ions have found extensive use in analytical chemistry in areas such as optical (particularly fluorescence) sensing,[2–5] and were, formerly, extensively used in gravimetric analysis of metals.[6,7] The 8-hydroxyquinolate (8-Hq) ligand is a selective sorbent of toxic metals.[8] Metal complexes of 8-Hq have also found biomedical applications, including tumour growth inhibitors in cancer treatment,[9,10] and as imaging agents in positron emission tomography (PET).[11] Supramolecular coordination compounds of 8-Hq and its derivatives are particularly promising for some of these applications.[12] However, probably the major use of metal quinolates at present is as light emitting and/or electron-transport layers in organic light emitting devices (OLEDs). This stems from the original observation of efficient electroluminescence from aluminium(III) quinolate (Alq_3) by Tang and van Slyke in 1987,[13] and forms the basis of a multi-billion Euro industry in displays for laptops, tablets and televisions. In addition to these applications, OLEDs are likely to be major candidates for the next generation of solid-state white lighting.[14] Electron transporting properties of aluminium quinolates also find applications in photovoltaic devices.[15]

The device efficiency of a molecule in these organic electronic systems depends on its highest occupied (HOMO) and lowest unoccupied molecular orbital (LUMO) energy levels. The development of Alq_3 as one of the most studied metal

---

[a] Centro de Química and Department of Chemistry, University of Coimbra, 3004-535 Coimbra, Portugal. E-mail: burrows@ci.uc.pt; Fax: +351-239827703; Tel: +351-239854482

[b] Department of Chemistry, University of Coimbra, 3004-535 Coimbra, Portugal

[c] CEMDRX, Department of Physics, University of Coimbra, 3004-516 Coimbra, Portugal

† Electronic supplementary information (ESI) available. See DOI: 10.1039/c5dt00727e

chelates for application in OLEDs stems from its high electron affinity (E_a) and ionization potential (I_p) values.[16] Cyclic voltammetry (CV) provides a convenient method to determine the oxidation and reduction potentials and, hence, the HOMO and LUMO levels in condensed phases. The oxidation process corresponds to the removal of one electron from the HOMO molecular orbital, so that the potential E_{ox} at which oxidation reaction occurs in CV is directly correlated with the energy required to extract the electron from the molecule. In a similar way, reduction peak potentials are used to determine the energy level of LUMO, which is the energy necessary to inject an electron into a molecule. The determination of HOMO and LUMO energies from CV data is achieved using the correlations discussed by Bredas *et al.*,[17] and expressed as:

$$E_{\mathrm{HOMO}} = -\mathrm{e}\ [E_{\mathrm{ox}} + 4.4], \tag{1}$$

$$E_{\mathrm{LUMO}} = -\mathrm{e}\ [E_{\mathrm{red}} + 4.4] \tag{2}$$

It is known that in an OLED, or other optoelectronic systems, the electron affinity (E_a) or E_{LUMO} level and the ionization potential (I_p) or E_{HOMO} level, relative to the cathode work function and the anode work function, respectively, determine the charge injection into the diode. Large energy barriers between HOMO and LUMO lead to poor OLED performance.[18] In addition, it has been demonstrated that the molecular orbitals localized on the hydroxyquinolate ligand are those that dictate the electroluminescence of Alq_3.[19]

However, these excellent electronic characteristics are tempered by the fact that Alq_3 degrades upon one-electron oxidation, which limits the long term stability of its optoelectronic devices.[20,21] Matrix assisted laser desorption/ionization time-of-flight mass spectrometry studies on Alq_3 show that ionization (*i.e.* one electron oxidation or hole formation) results in ligand loss to form the Alq_2^+ species, which may undergo dimerization or other processes.[22] Although in the thin layers involved in solid state devices, the ligand cannot readily diffuse through the film layers, allowing the possibility of its recombination with the Al(III) centre, in the long term, the instability of the radical cation will lead to degradation and a decrease in the device lifetime. There is, thus, a strong incentive for developing alternative materials.

Chromium(III) and aluminium(III) have very similar ionic radii and coordination numbers (typically six), and their complexes have comparable thermodynamic stabilities.[23] There are, however, two important differences. Firstly, while aluminium only shows a single stable trivalent oxidation state (Al(III)), the chromium metal ion can exist in a wide variety of oxidation states, with the one electron oxidized (Cr(IV)) and reduced (Cr(II)) states obtained from chromium(III) being stable and readily accessible, in energetic terms.[24] In addition, while Al(III) complexes fairly rapidly undergo ligand exchange, the $3d^3$ electronic configuration of chromium(III) makes its complexes kinetically inert to substitution, with rates at least a million times slower than those of the corresponding aluminium(III) complexes.[23,25,26]

Chromium(III) complexes also show interesting electronic spectral properties, involving metal based quartet and doublet states, together with ligand based π,π* states, and, possibly, charge transfer states, as demonstrated by detailed UV/visible absorption,[27] luminescence spectra,[28,29] and photophysical studies.[30,31] In one case, electrogenerated chemiluminescence has been observed with a chromium(III) complex.[32] The above characteristics make chromium(III) quinolates good candidates for further study for optoelectronic applications.

Further interest in stable chromium(III) complexes stems from their paramagnetic character. The development of nuclear magnetic resonance image techniques as a clinical diagnostic modality has prompted the need for a new class of pharmaceuticals to enhance the image contrast between normal and diseased tissue or indicate the status of organ function or blood flow. The image intensity in ^1H NMR imaging, largely composed of the NMR signal of water protons, is dependent on nuclear relaxation times. Complexes of lanthanide ions, *e.g.* Gd(III), which can decrease the relaxation times of nearby nuclei *via* dipolar interactions, have received the most attention as contrast agents.[33,34] The important properties related with the ^1H fast relaxation of nearby nuclei of the Cr(III) complexes and their spherical symmetry may also make them good potential candidates for use as relaxation agents having potential application in magnetic resonance imaging (MRI).

For the above reasons, we have carried out a detailed structural, spectral and electrochemical study on chromium(III) 8-hydroxyquinolate (Crq_3). Although chromium(III) 8-hydroxyquinolate was first reported in 1938,[35] reliable results on its synthesis and characterization have been fairly sporadic,[6,36–44] and it is only recently that relatively detailed structural data on this compound have been reported.[45] In part, this stems from the same kinetic inertness that makes this material interesting for device applications. In addition, Crq_3 tends to crystallize as a solvate.[36,46] Following from our earlier studies on the water soluble derivative 8-hydroxyquinoline-5-sulfonate (8-HqS) with the trivalent cations Al(III),[47,48] we initially studied standard routes to Crq_3 synthesis by looking at the reaction of the water soluble 8-HqS with chromium(III) in aqueous solutions. However, no significant reaction was observed over several weeks,[49] in support of the kinetic inertness of the Cr(III) ion. Considering the reported routes to Crq_3, the method used by Li *et al.* involved reacting chromium nitrate and 8-hydroxyquinoline in the presence of gadolinium(III) nitrate.[45] However, since the presence of trace quantities of Gd(III) may have adverse effects on the spectral and magnetic properties of Crq_3, we have opted for adaption of another literature method involving reaction of chromium(III) and 8-hydroxyquinoline in the presence of urea and ammonium chloride/acetic acid buffer.[38,50] The product has been characterized by elemental analysis, mass spectrometry, thermogravimetry, FTIR, ^1H NMR spectroscopy, and X-ray powder diffraction. Additional information on both geometric and electronic structure has come from density functional theory (DFT) calculations, and UV/Visible absorption and diffuse reflectance spectra. Preliminary studies on its luminescence have also been made. These are complemented by detailed cyclic voltammetry studies on Crq_3, Alq_3 and the ligand 8Hq. Comparison of CV and electronic spectral data with results from DFT calculations provides details on both structure and electronic properties, which are used as a framework to assess the potential of this system for optoelectronic applications.

2. Experimental

2.1. Reagents

Chromium nitrate hexahydrate ($Cr(NO_3)_3 \cdot 6H_2O$) was purchased from Merck, and 8-hydroxyquinoline was obtained from Aldrich and used without further purification. Synthesis of the Alq_3 sample used has been described elsewhere.[51] All solvents were of the highest purity commercially available and, where appropriate, were further purified by literature procedures.

2.2. Synthesis of Crq_3 by the urea method

This is based on a literature procedure.[38,50] The product was recrystallized in a water/methanol mixture (10 : 90%) by slow evaporation at room temperature. A brown powder was obtained after one week. Yield: 80% (based on Cr ions). The precipitate is soluble in common organic solvents such as acetone, benzene, chloroform or alcohol. Elemental analysis (%): C 65.08 (expected for $CrC_{27}H_{18}N_3O_3$: 66.94; expected for $CrC_{27}H_{18}N_3O_3 \cdot CH_3OH$: 65.11); H, 4.35 (expected for $CrC_{27}H_{18}N_3O_3$: 3.75; expected for $CrC_{27}H_{18}N_3O_3 \cdot CH_3OH$: 4.29); N, 8.02 (expected for $CrC_{27}H_{18}N_3O_3$: 8.67; expected for $CrC_{27}H_{18}N_3O_3 \cdot CH_3OH$: 8.14) is fully consistent with the product being a methanol solvate of Crq_3.

2.3. Equipment and methods

Mass spectra were recorded using a MALDI-TOF, Voyager-DE™ PRO Workstation, with positive reflector mode acquisition.

Carbon, hydrogen and nitrogen elemental analyses were performed in duplicate at the Servicio de Análisis Instrumental – Unidad de Anãlisis Elemental, CACTI Vigo, Universidad de Vigo, Spain.

Thermogravimetry was performed using a Netzsch thermal analyzer, TG 209 F3, over the range 30–900 °C under a dynamic N_2 atmosphere with a heating rate of 10 °C min^{-1}. The chromium content was determined by igniting a known weight of the dried precipitate and weighing the chromium(III) oxide.

The Fourier Transform-Infrared Spectroscopy (FTIR) was carried out over the range 4000–400 cm^{-1} with resolution of 1 cm^{-1} on samples in KBr pellets using a Nicolet FT-IR 6700 spectrophotometer, or using an ATR Smart Orbit ATR Diamond Attenuated Total Reflectance (ATR) accessory with a Thermo Nicolet 380 FTIR spectrometer.

The ^1H NMR spectra were obtained using a Varian Unity-500 NMR spectrometer (at 499.843 MHz), using sw = 41 972.72 Hz, tof = 67.38 Hz, at = 1.5 s, d1 = 0.2 s. The methyl signal of *tert*-butyl alcohol and the DMSO signal were used as internal references for ^1H, in D_2O (δ 1.3 ppm relative to TMS) and in DMSO (δ 2.5 ppm relative to TMS) solutions, respectively.

X-ray powder diffractograms were obtained using an ENRAF-NONIUS FR590 powder diffractometer equipped with an INEL120 detector (Debye–Scherrer geometry) using CuKα radiation. The powder was used to fill a glass capillary, which was slowly rotating upon data collection. Calibration was performed using silicon as an external calibrant.

Cyclic voltammetry (CV) measurements were performed on a computer-controlled μ-Autolab type I potentiostat–galvanostat with GPES software (Metrohm-Autolab, Utrecht, Netherlands). The experiments were carried out in acetonitrile (ACN) containing 0.1 M tetra-*n*-butylammonium perfluorate (TBAP) as a supporting electrolyte. A three-electrode system was used and consisted of a glassy carbon working electrode (1 mm diameter), a platinum wire counter electrode, and an Ag/AgCl reference electrode. Peak currents were measured from extrapolation of the baseline just before the peaks in the cyclic voltammograms.

UV–Visible absorption spectra in solution were recorded over the range 200–800 nm using a Shimadzu UV-2010 double-beam spectrometer, with samples in 1 cm quartz cuvettes. Diffuse reflectance (DRS-UV–vis) spectra of solid samples were recorded over the range 300–800 nm using a Shimadzu UV-2450 double-beam spectrometer with an integrating sphere, using barium sulfate as a reference material.

Photoluminescence (PL) excitation and emission data were collected on samples in solution in 1 cm quartz cuvettes using a Spex Fluorolog 3-22 spectrophotometer, using a 300 W xenon arc lamp as an excitation source.

2.4. DFT computational details

The molecular structures of the open shell d^3 (quartet state) meridional and facial Crq_3 isomers were optimized using the GAMESS-US code[52] at the DFT level using the B3LYP (Becke three-parameter Lee–Yang–Parr)[53,54] exchange correlation functional. The geometries were optimized without symmetry constraints in the case of the meridional structure (C_1 point group) and constraining the symmetry to the C_3 point group in the case of the facial isomer. The calculations were performed using both the restricted open-shell (RO-B3LYP) and the unrestricted (U-B3LYP) formalisms. In the case of the U-B3LYP calculations, spin-contamination was assessed by a comparison of the expected $S(S+1)$ for the assigned spin state and the actual value of $\langle S^2 \rangle$. The Stuttgart relativistic small core (RSC) 1997 valence and effective core potential (ECP) functions[55] were used for the metal, and the 6-311G(d,p) basis sets were used for the expansion of the Kohn–Sham orbitals of the ligand atoms. The bulk solvent (DMSO or acetonitrile) effects were taken into account through the polarizable continuum model (PCM) of Tomasi and co-workers.[56,57] Default van der Waals radii were used for all atoms except for chromium, for which 2.36 Å was used. The Hessian was calculated for the resulting stationary points, and the geometries were characterized as true minima (*i.e.*, no imaginary frequencies). The gradient threshold for geometry optimization was taken as

10^{-5} Hartree per Bohr. The geometries of the cation Crq_3^+ (d^2 configuration, triplet state) and of the anion Crq_3^- (d^4 configuration) of the meridional isomer were also optimized using the same methods as for the neutral molecules. The ionization energy (I_p) and the electron affinity (E_a) were calculated as the difference between the ground state energies of the corresponding charged states and the neutral molecule, $I_p = E(+1) - E(0)$ and $E_a = E(0) - E(-1)$.[58] The calculations on the anion were done assuming a high spin system (a system in which the additional electron occupies the LUMO orbital, therefore a quintet state). Additionally, the geometry of the anion and the neutral meridional isomer were also optimized using the 6-31+G(d) basis sets, which include diffuse functions to better represent the extra charge in the anion.

3. Results and discussion

3.1. Synthesis and characterization

As indicated in the Experimental section, the compound was synthesized by adapting a literature method,[38,50] involving a reaction between chromium(III) (as its nitrate) and 8-hydroxyquinoline in an acetic acid/ammonium chloride/ammonium acetate buffered solution. The solid product was recrystallized from a water/methanol mixture (10 : 90%) by slow evaporation at room temperature. Brown crystals appeared after several days (m.p. >300 °C). As indicated in the Experimental section, the C, H, N elemental analysis is consistent with formation of the methanol solvate of Crq_3.

Confirmation of the formation of Crq_3 came from the MALDI-TOF mass spectrum (Fig. 1), where a clear molecular ion peak located at $m/z = 484.0408$ is observed, corresponding to Crq_3^+ (theoretical value for $CrC_{27}H_{18}N_3O_3^+$ from isotopic masses $m/z = 484.0753$).[59] Additional peaks located at $m/z = 507.0490$ and 523.0234 were observed, and may correspond to $[M + Na]^+$ and $[M + K]^+$, respectively. This contamination is probably due to the glass in contact with this type of sample, and is fairly common for organic compounds with an affinity for alkali metal cations.

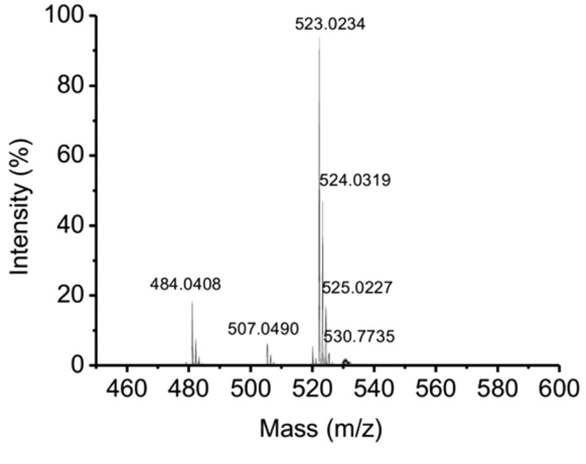

Fig. 1 MALDI-TOF mass spectrum of Crq_3.

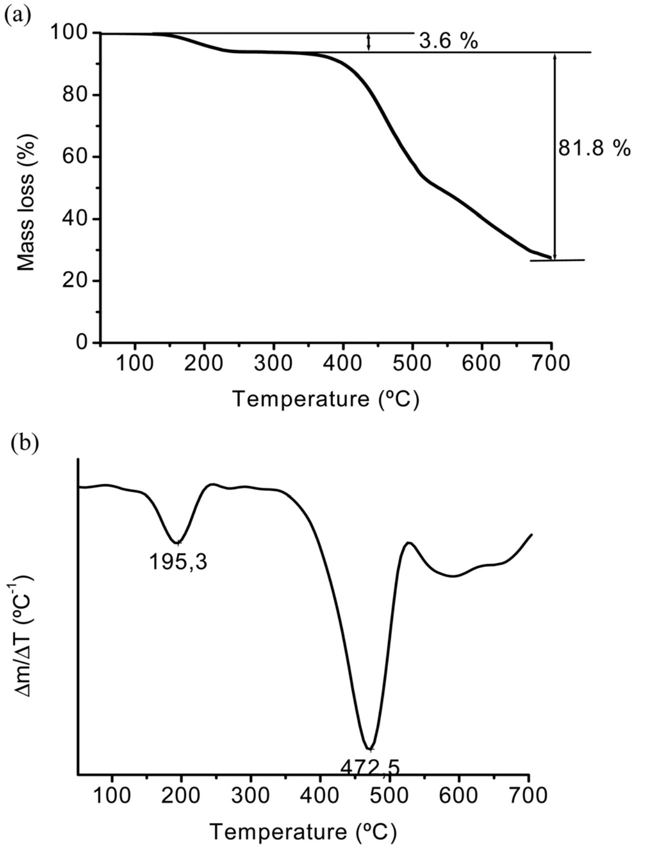

Fig. 2 (a) Thermogravimetric analysis of Crq_3 under a nitrogen atmosphere; (b) differential thermogram.

The complex was also analysed by thermogravimetry (Fig. 2), which showed an initial small weight loss around 200 °C, a second step around 470 °C, and final weight losses between 500 and 700 °C. Previous studies on Crq_3[36,46] and the corresponding cobalt(III) derivative[60] show that they tend to crystallize as alcohol adducts, with the solvent trapped in a "cage-like" cavity, and that the alcohol can be eliminated upon heating around 200 °C. From the thermogravimetric data, and C, H, N elemental analysis, we suggest that with our synthesis, the Crq_3 recrystallizes from 90% methanol–water with similarly trapped methanol molecules, and that these are lost in this first stage of heating. As we will see shortly, support for this comes from both FTIR and ^1H NMR spectra. Results in Table 1 show that the subsequent loss in weight is fully consistent with a stoichiometry involving three molecules of 8-hydroxyquinolate per atom of chromium. Ignition at *ca.* 470 °C for 1 h quantitatively converts the complex to chromium(III) oxide (Cr_2O_3) (Fig. 2). The residual mass confirms the presence of the oxide, and the thermal behaviour is similar to that of other metal quinolates.

Solid samples of the product were analysed by FTIR spectroscopy, both as KBr disks and using attenuated total

Table 1 Thermogravimetric characteristics of Cr(III) complex

Complex	Temp. range (°C)	Mass loss (%) (exp.)	Assignment	Residue
$[C_{27}H_{18}N_3O_3Cr]\cdot 0.5CH_3OH$	50–250	3.6	$0.5CH_3OH$	$1/2Cr_2O_3$
	300–800	81.8	$C_{27}H_{18}N_3O_3$	

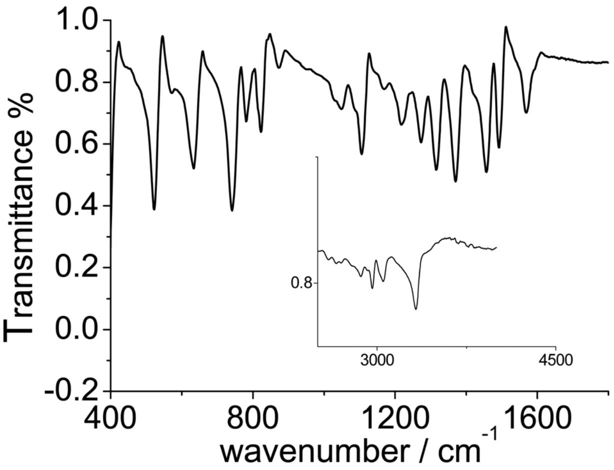

Fig. 3 FTIR spectrum of solid recrystallised from 90% methanol–water (inset shows the 2500–4500 cm^{-1} region).

reflectance (ATR). The only significant difference observed between spectra obtained using these different sampling techniques was in the 3000–3600 cm^{-1} region, probably due to the presence of trace water in the KBr discs. The ATR spectrum is shown in Fig. 3. All the characteristic bands observed in the IR spectra of the solid are presented in the ESI (Table S1†), and are discussed in relation to the structure Crq$_3$ on the basis of literature data on various metal 8-hydroxyquinolates.[37,61–65] The observation of an absorption around 3325 cm^{-1} and sharp bands at 2959 and 2866 cm^{-1} are attributed to methanol,[66] and are in complete agreement with the TG data of occluded solvent within the solid Crq$_3$. These are markedly reduced in intensity on heating the sample to 200 °C, in agreement with methanol loss on heating.

Further information on the structure was obtained by ^{1}H NMR spectroscopy. In this discussion we use the numbering of the ring positions of 8-hydroxyquinoline (8-Hq) indicated below (Scheme 1).

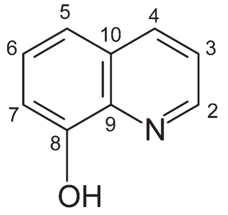

Scheme 1 Structure of 8-hydroxyquinoline (8-Hq).

8-Hq is known to form extremely stable bidentate chelate complexes with the most transition and main group metal cations. The ^{1}H NMR spectra of 8-Hq as well as the ^{1}H signals of the water soluble derivative 8-HqS have previously been assigned in the literature.[4,67]

For the determination of structural features of the complex Cr(III)/8-Hq in solution, we obtained the ^{1}H NMR spectra of both 8-Hq and the synthesized complex Crq$_3$ in DMSO-d_6. Results are illustrated in Fig. 4 for the ^{1}H NMR spectra of 8-Hq and the complex Crq$_3$. The complete ^{1}H NMR spectral parameters for 8-Hq and its complexes with Cr(III) are shown in Table 2. In addition, the spectrum of Crq$_3$ shows a broad band at 3.33 ppm attributed to methanol, in agreement with the thermogravimetry and FTIR results on the presence of this solvent.

The complexes are paramagnetic and, because of the rapid relaxation time caused by the paramagnetic properties of the Cr(III) metal ion, ^{1}H NMR signals of bound ligands (inner sphere) are observed to be dramatically broadened and shifted to high frequencies (Fig. 4 and Table 2). Based on the mass spectral and TG data, this is assumed to be a species with a 1 : 3 (metal : ligand) stoichiometry.

Fig. 5 shows the comparison of the envelope signals for Crq$_3$ and Alq$_3$, which also suggest that these complexes are homologous. Although the comparison of the ^{1}H NMR spectra of the paramagnetic complexes Crq$_3$ with the ^{1}H NMR spectra of the diamagnetic Alq$_3$ (Fig. 5) suggests a rough attribution, the large widths of the bound ligand resonances (metal ion inner sphere) of the Crq$_3$ complex precludes the complete assignment of the signals. However, the dramatic shifts observed are in accordance with similar effects observed in previous studies on the acetylacetonate complex of Cr(III).[68,69]

Shifts as a result of ligand binding to paramagnetic metals may come either from through-space dipolar interactions (pseudo-contact), or from direct delocalization of unpaired electron spin-density from the metal (contact shift). The Cr(III) metal ion in the complex mainly produces a contact shift, which implies that the electron spin is partly delocalized between the 3d orbitals of the metal atom and the π orbitals of the ligand. Comparison with the behavior of chromium(III) acetylacetonate complexes[68] suggests that this involves ligand donation to the empty e orbitals of the metal. As we see later, this is fully consistent with the DFT description of the electronic structure of the complex. The potential of Crq$_3$ as a paramagnetic NMR relaxation agent is discussed in the ESI.†

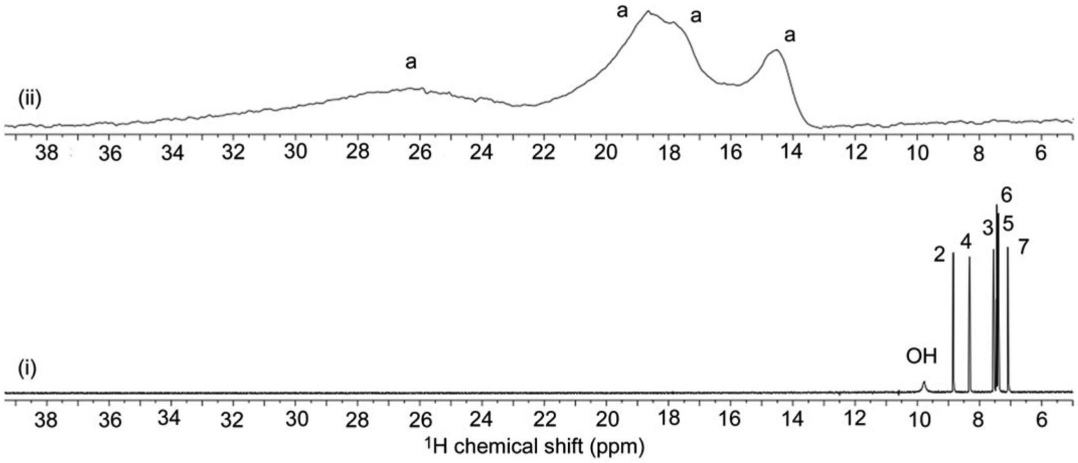

Fig. 4 ^{1}H NMR spectra (499.824 MHz) obtained from −30 to 50 ppm of DMSO-d_6 solutions of (i) 8-Hq 10 mmol dm^{-3}, and (ii) Cr(III)/8-Hq complex 10 mmol dm^{-3}.

Table 2 ^{1}H NMR parameters[a] for 8-Hq and its complexes with Cr(III) (298 K)

	H–2	H–3	H–4	H–5	H–6	H–7	O*H*	$J_{2,3}$	$J_{3,4}$	$J_{2,4}$	$J_{5,6}$	$J_{6,7}$	$J_{5,7}$
8-Hq[b] (δ)	8.85	7.55	8.32	7.39	7.44	7.08	9.77	4.2	8.3	1.7	7.5	7.5	1.4
Cr(III)/8-Hq[c] complex (δ)	25.0/18.6/17.6/14.4						—[d]	—[e]	—[e]	—[e]	—[e]	—[e]	—[e]

[a] δ values, in ppm, relative to Me$_4$Si, using the signal of DMSO as an internal reference (δ 2.5 ppm); *J* values in Hz. [b] Solution of 8-Hq 10 mmol dm^{-3} in DMSO-d_6. [c] Complex synthesized according to the experimental procedure. [d] Not detected. [e] Not observed.

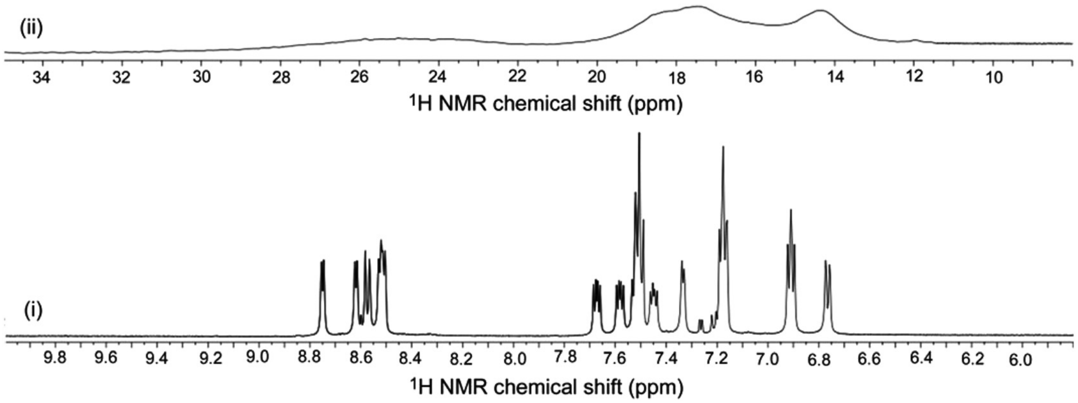

Fig. 5 ^{1}H NMR spectra (499.824 MHz) obtained from −30 to 50 ppm of (i) a D_2O solution of Al(III)/8-Hq (Alq$_3$) 10 mmol dm^{-3}, and (ii) a DMSO-d_6 solution of Cr(III)/8-Hq (Crq$_3$) complex 10 mmol dm^{-3}.

Finally, the structure of the solid product was characterized by X-ray powder diffraction (Fig. 6). As seen by the great similarity between the experimental powder diffractogram and that simulated from the data reported by Li *et al.*[70] using PLATON,[71] one can state that the main features of the supramolecular organization are common to both compounds. Most likely, our compound is a tris(8-quinolinate) chromium(III) methanol solvate almost isostructural with the already reported ethanol solvate.[46] Li *et al.* describe their complexes as having three 8-quinolinate ligands chelating to each Cr(III) ion in a octahedral geometry.[70] They observed short distances between the aromatic rings of neighboring complexes and presumed π–π interactions as one of the key factors regulating the supramolecular assembling. The ethanol solvent molecules are H-bonded to the metal complexes through the quinolate oxygen atom. The solvent molecules (four in each unit cell) occupy two large voids of 186 Å.

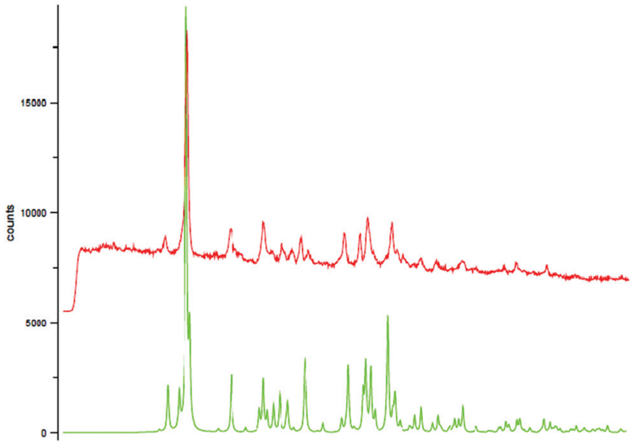

Fig. 6 X-ray powder diffractogram of the solid product. Top (in red) experimental powder diffraction. Bottom (in green) simulated powder diffractogram for Crq_3 methanol solvate.

3.2. DFT studies

To help elucidate the coordination mode of Cr^{3+} with 8-Hq, the structures of the meridional and facial isomers of the complex were optimized at the DFT level and their relative energies were determined. The results from the RO-B3LYP calculation indicate that the meridional isomer is more stable than the facial isomer by 10.56 kJ mol^{-1} (10.71 kJ mol^{-1} in the U-B3LYP calculation). The equilibrium geometry with minimum energy of the *mer*-[Crq_3] complex is shown in Fig. 7 and selected geometrical parameters are given in Table 3.

As expected due to the *trans* effect, the longest Cr–N bond is Cr–N_I, which is opposite to the shortest Cr–O bond (Cr–O_{III}).

The LUMO in the complex is essentially localized on the ligands, but still has some charge on the metal (*i.e.* on the metal d_{z^2} orbital). In contrast, the HOMO corresponds essentially to one of the t_2 metal orbitals (with some minor charge localized on the ligands) (Fig. 8). This has important implications regarding the oxidation and reduction processes, which are relevant for charge injection in devices, as we discuss later. The ionization energy of the complex was estimated using two different approaches. First, we considered the DFT counterpart of Koopmans' theorem, which states that the first vertical ionization energy is equal to the negative of the energy of the highest occupied molecular orbital (HOMO). This is not entirely valid for the restricted open-shell orbitals; therefore we have considered the unrestricted calculation in this approach. In a second approach, we have calculated the ionization energy as the difference between the ground state energies of the positive ion and the neutral molecule, $I_p = E(+1) - E(0)$. This was done either keeping the geometry fixed

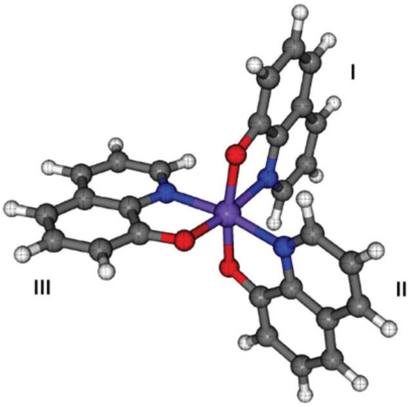

Fig. 7 Optimized RO-B3LYP geometry of the *mer*-[Crq_3] complex.

Table 3 Selected bond lengths (Å) and angles (degrees) calculated at the RO-B3LYP/6-311G(d,p) level in PCM (DMSO)[a] for the *mer*-[Cr(Hq)$_3$] complex

Bond lengths		Angles	
Cr–O_I	1.973	O_I–Cr–N_I	79.76
Cr–O_{II}	1.986	O_{II}–Cr–N_{II}	81.03
Cr–O_{III}	1.959	O_{III}–Cr–N_{III}	81.19
Cr–N_I	2.119	O_I–Cr–O_{II}	170.27
Cr–N_{II}	2.081	N_I–Cr–O_{III}	172.45
Cr–N_{III}	2.102	N_{II}–Cr–N_{III}	169.33

[a] Polarizable continuum model.[56,57]

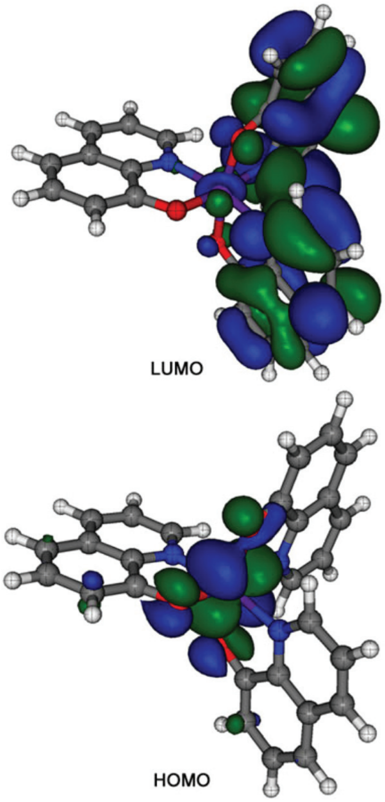

Fig. 8 Highest occupied (HOMO) and lowest unoccupied (LUMO) molecular orbitals for the *mer*-[Crq_3] complex calculated at the RO-B3LYP/6-311G(d,p) level of theory.

in the neutral ground state geometry (vertical ionization energy), or at the optimized geometries of both the charged and neutral species (adiabatic ionization energy). In these calculations, the bulk effects of the solvent (DMSO or acetonitrile) were taken into account through the polarizable continuum model.[56,57] Using the first approach, and considering DMSO as the solvent, we obtained a value of 5.47 eV for the ionization energy, and using the second approach we obtained 5.63 and 5.95 eV for the adiabatic and vertical ionization energies, respectively. Changing the solvent from DMSO to acetonitrile had a negligible effect on the vertical ionization energy, which only increased to 5.96 eV.

The accurate computation of the electron affinity is more difficult because the correct calculation of the structure and energy of the anion is strongly dependent on the basis set used. Additionally, the negative of the lowest unoccupied molecular orbital (LUMO) energy in the neutral system is not a good estimate for the electron affinity.[72] A rather better approximation is to use the negative of the energy of the additional occupied orbital in the anion. Using this approach, we obtained a value of 2.45 eV for the U-B3LYP calculation of the anion with the 6-311G(d,p) basis set and 2.51 eV using the 6-31+G(d) basis set. Additional calculations using the $E_a = E(0) - E(-1)$ approach gave the value of 2.23 eV for the adiabatic electron affinity calculated at the U-B3LYP level with the 6-31+G(d) basis set.

3.3. Cyclic voltammetry

Cyclic voltammetry has been performed on Crq_3, Alq_3 and, for comparison, on the free ligand 8-Hq in acetonitrile solutions using a three-electrode system consisting of a glassy carbon working electrode, a platinum wire counter electrode, and an Ag/AgCl reference electrode. The results are shown in Fig. 9 and 10. The quinolate solutions were prepared and stored in the fridge in between use. The same voltammetric profiles were recorded when using the prepared quinolate solutions over more than 2 months, which indicates the high stability of the compounds in acetonitrile.

The compound Crq_3 presents 4 oxidation peaks in the positive region in the first scan, and two corresponding, less intense reduction waves and in the negative region two pairs of reversible peaks. The oxidation peaks are located at 0.85, 1.18, 1.42 and 1.60 V *vs.* Ag/AgCl with peak currents of 350, 150, 150, and 380 μA cm^{-2} for peaks 1, 2, 3 and 4, respectively. The corresponding reduction waves, which, unlike the oxidation ones, are of constant height on cycling the potential, are situated at 0.84 and 1.53 V *vs.* Ag/AgCl with very small current densities of 88 and 40 μA cm^{-2}, respectively.

Oxidation peak 1 merges with peak 2, and shifts towards more positive potentials upon cycling, from 0.85 to 1.13 V, at which potential it stabilizes. Peaks 3 and 4 merge during the second scan and form a broader peak with a similar current intensity at 1.50 V. This merged peak decreases drastically in scan 3, and then splits to form peaks 3 and 4 again during further CV scans. After 4 scans, the CV profile contains 3 oxidation peaks at 1.13, 1.41 and 1.53 V *vs.* Ag/AgCl, with peak currents of 330, 120 and 150 μA cm^{-2}, respectively.

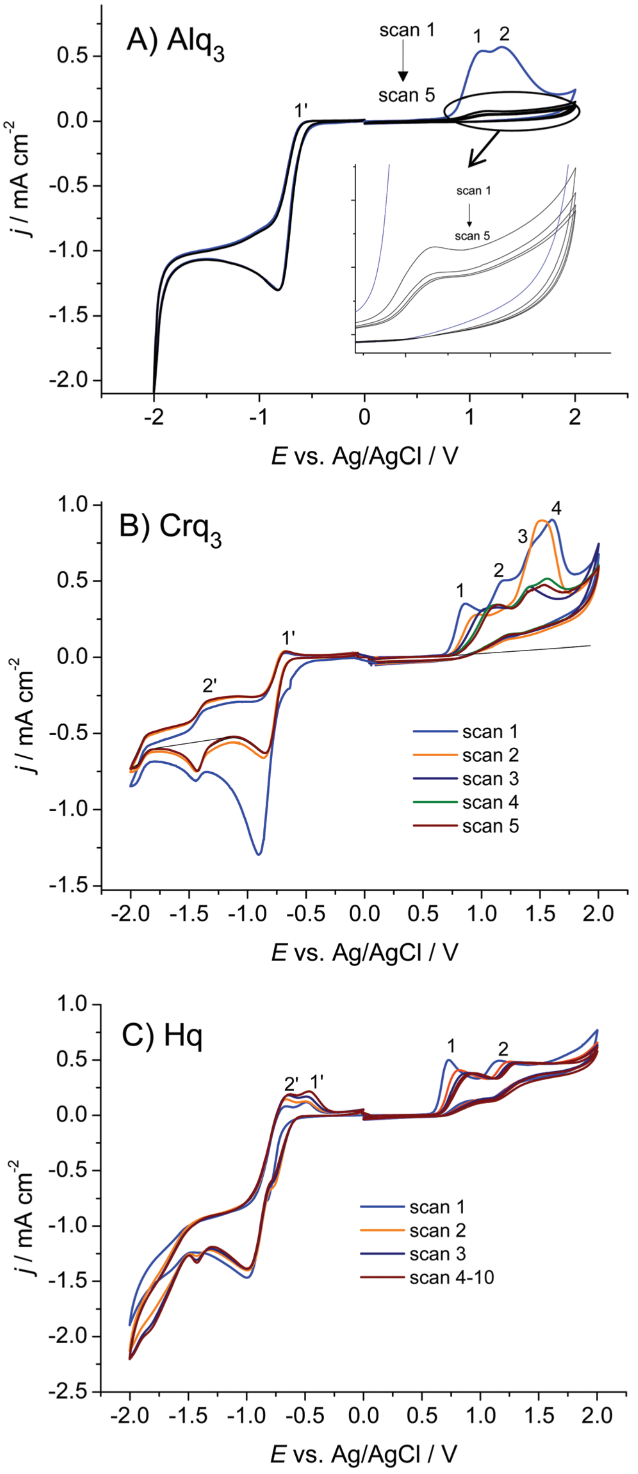

Fig. 9 Cyclic voltammograms recorded at (A) Alq_3, (B) Crq_3, and (C) 8-Hq in 0.1 M TBAP in ACN at v = 50 mV s^{-1}.

In the negative region, two pairs of reversible peaks appear with midpoint potentials of −0.76 and −1.40 V *vs.* Ag/AgCl. The oxidation peaks remain constant with potential cycling,

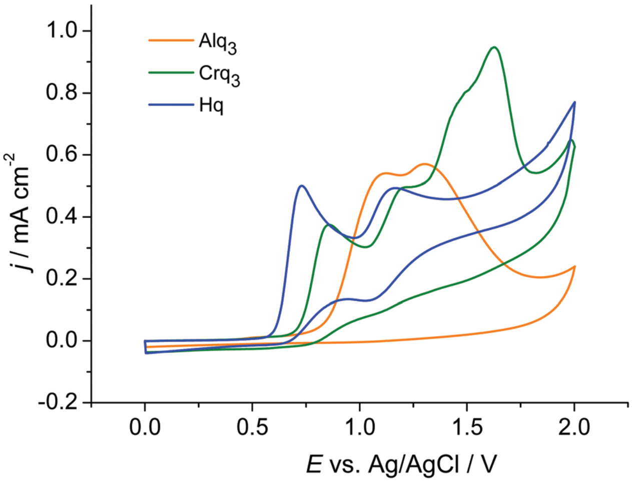

Fig. 10 Cyclic voltammograms (first scan) recorded in the positive potential region at Alq_3, Crq_3, and 8-Hq in 0.1 M TBAP in ACN at v = 50 mV s^{-1}.

while the reduction peak current 1′ decreases to half the value in scan 2, from 1260 to 580 μA cm^{-2}, and then remains constant. Reduction peak 2′ becomes better defined in the second and following CV-s, and the peak current increases from 130 to 230 μA cm^{-2}.

The compound Alq_3, in the first CV scan, presents two irreversible oxidation peaks in the positive region, which, as in the case of Crq_3, then merge into one peak with considerably reduced currents, and shows one pair of peaks in the negative region, which remained unchanged during cycling. The oxidation peaks 1 and 2 appear at the potentials E_{ox1} = 1.11 V and E_{ox2} = 1.31 V *vs.* Ag/AgCl, with peak currents j_{ox1} = 550 and j_{ox2} = 570 μA cm^{-2}, respectively. During cycling, these two peaks merge into one at 1.18 V, with a lower current of 50 μA cm^{-2}. The fact that, after polishing the electrode to have a clean electrode surface, the two peaks in scan 1 reappear with similar current densities, indicates that oxidation products or by-products may cover the electrode, leading to the decrease in current in second and subsequent cycles. In the negative region, a quasi-reversible reaction occurs, with midpoint potential of −0.70 V, with $j_{red1'}$ = 1300 μA cm^{-2} and $j_{ox1'}$ = 840 μA cm^{-2}.

For comparison, studies were carried out on the free ligand, 8-Hq, which presents two oxidation peaks in the positive region in the first cycle with two small reduction waves, and one reduction and two oxidation peaks in the negative region. The oxidation peaks in the positive region are situated at 0.73 and 1.16 V *vs.* Ag/AgCl, with peak currents of 500 and 150 μA cm^{-2}. After 5 cycles, these oxidation peaks are shifted towards more positive potentials of 0.93 and 1.31 V *vs.* Ag/AgCl, with lower constant currents of 350 and 130 μA cm^{-2}. In the negative region, there is one main reduction peak during the first scan at −0.98 V, height 1470 μA cm^{-2}, and a small shoulder at −0.77 V. Upon cycling, the shoulder at −0.77 V becomes bigger, and a small new peak appears at −1.42 V, with a peak current of 120 μA cm^{-2}, together with a new, less evident reduction wave at −1.90 V *vs.* Ag/AgCl. The main reduction peak decreases slightly from 1470 to 1360 μA cm^{-2}, from the first to the last cycle.

The oxidation peaks 1′ and 2′ are situated at −0.48 and −0.69 V, with peak currents of 790 and 820 μA cm^{-2}, which slightly increase with potential cycling to 900 and 920 μA cm^{-2}.

Full details are summarized in Tables 4 and 5.

The first two peaks observed in the CVs of Alq_3 are related to 8-Hq. Peak number 1 is irreversible, and is attributed to the formation of $–O^{\bullet}$ radicals,[73] and the second, which is quasi-reversible, to the formation of a quinoid-like structure, as presented in Scheme 2. With Alq_3, the oxidation potentials are shifted to more positive values than those of 8-Hq, since the oxygen atom of the ligand covalently binds the central metal ion, which makes its oxidation more difficult. As has previously been reported, with Alq_3, the oxidations are irreversible.[74] In the case of Crq_3, the first peak is at 0.85 V, while further peaks are seen at 1.18, 1.42 and 1.60 V. The oxidation is more reversible in this case than with Alq_3, in agreement with our prediction. With potential cycling, for both complexes, peaks 1 and 2 merge into one peak, at 1.18 and 1.13 V *vs.* Ag/AgCl, respectively, having different current densities, markedly lower for Alq_3 (50 μA cm^{-2}) than for Crq_3 (330 μA cm^{-2}). The decrease in the oxidation peak currents in the positive region after the first 2 cycles is, in both cases, related to the passivation of the electrode by the decomposition products of the quinolates. Nevertheless, this decrease is significantly greater in the case of Alq_3, which clearly indicates that Crq_3 does not decompose as much as Alq_3.

Table 4 Oxidation potentials extracted from the CVs for the compounds Alq_3, Crq_3, and 8-Hq

		E/V *vs.* Ag/AgCl				*j*/μA cm^{-2}			
Compound	Scan no.	Ox1	Ox2	Ox3	Ox4	Ox1	Ox2	Ox3	Ox4
Alq_3	1	1.11	1.31	—	—	550	570	—	—
	10	1.18		—	—	50		—	—
Crq_3	1	0.85	1.18	1.42	1.60	350	150	150	380
	10	1.13		1.41	1.53	330		120	150
8-Hq	1	0.73	1.16	—	—	500	150	—	—
	10	0.93	1.31	—	—	350	130	—	—

Table 5 First oxidation/reduction potentials, and corresponding I_p and E_a, and gap energy E_g extracted from the CVs for the compounds Alq_3 and Crq_3

	E_{ox}/V	$-I_p$ (E_{HOMO})/eV	E_{red}/V	$-E_a$ (E_{LUMO})/eV	E_g/eV
Alq_3	1.11	−5.51	>−2.0[a]	>−2.40	>3.11
Crq_3	0.85	−5.25	−1.37	−3.03	2.22

[a] E_{red} of Al^{3+} probably occurs at more negative potentials, out of the potential range of the electrode.

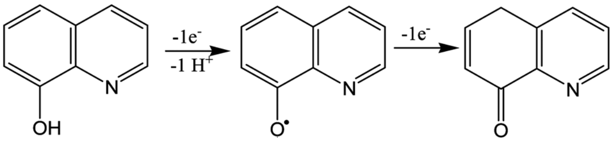

Scheme 2 Oxidation mechanism of 8-Hq.

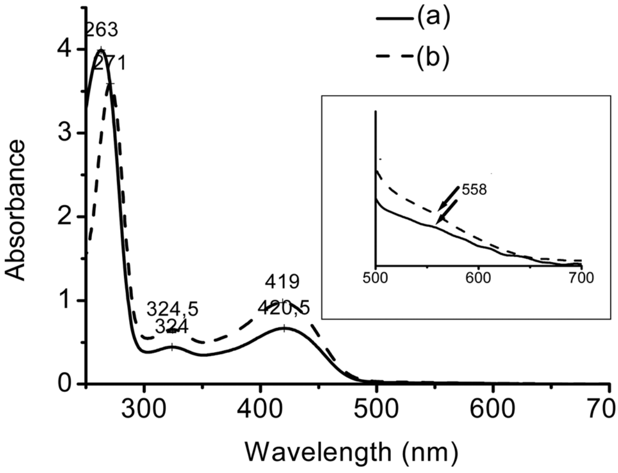

Fig. 11 UV/Visible absorption spectra of Crq_3 in (a) dichloromethane and (b) dimethylsulfoxide (inset: region between 500–700 nm).

The peaks 3 and 4 for Crq_3 are attributed to formation of higher metal oxidation states.

The HOMO and LUMO energies, together with the HOMO–LUMO separation (E_g) were calculated from the oxidation and reduction potentials using the expressions given in eqn (1) and (2). For Alq_3, the HOMO energy is in excellent agreement with the literature value of −5.65 eV.[75] The LUMO energy cannot be measured directly because it is outside the potential range of the GCE in organic media, but is fully consistent with literature values of −2.90 V[75] and −3.0 V.[16]

For Crq_3, the HOMO energy is close to the value −5.47 eV calculated considering the DFT counterpart of Koopmans' theorem, with the solvent included. The value is also in reasonable agreement with that calculated for the adiabatic ionization energy from the difference in ground state energies between the positive form and the neutral molecule, at their optimized geometries (−5.63 eV). This provides strong support to the idea from the DFT calculations that the HOMO is mainly localized on one of the metal d orbitals. The agreement between the LUMO energy obtained by CV (−3.03 eV) and that obtained by DFT (for example, −2.51 eV using the 6-31+G(d) basis set) was less good. However, we discussed earlier the difficulties in the accurate calculation of electron affinity in these systems. Similar underestimation of LUMO energies in DFT calculations have previously been reported for Alq_3.[75]

3.4. UV/Visible absorption and luminescence spectral studies

The UV/Visible absorption spectra for complex Crq_3 in two solvents, dichloromethane and dimethylsulfoxide, are essentially identical, and are shown in Fig. 11. Two intense absorption bands at approximately 270 and 420 nm dominate the spectrum. These are reminiscent of the corresponding bands in the *mer* isomer of Alq_3[76] and, based on this can be assigned to the ligand centred electronic transitions. In addition to these intense bands, there is a weak absorption band at 324 nm, which may be part of a vibronic progression associated with the deformation mode.[76] In the region between 500–700 nm, there is a broad, low intensity shoulder at *ca.* 558 nm. Although not observed in a recent report on this compound,[43] probably because the solutions used were too dilute, this band was seen in early studies on Crq_3,[36] and can be attributed to a d–d transition of the chromium ion. These bands have low molar absorption coefficients, ε, because they are Laporte "forbidden" transitions. The observation of this band is in complete agreement with the DFT results indicating that the HOMO is mainly localized on the metal t_2 orbital. Based on literature data on related chromium(III) complexes[27] the 558 nm band is attributed to the $^4A_2 \rightarrow {}^4T_2$ transition. We note the absence of any $n \rightarrow \pi^*$ band, in agreement with the formation of the metal–nitrogen bond, with the quinolate complex stabilizing the electron pair on the nitrogen atom.[77] The energy of this shoulder (2.22 eV), which corresponds to the HOMO–LUMO gap, is identical to that determined by CV. Whilst the perfect agreement is, possibly, fortuitous, it fully supports the assignment of the HOMO to a metal based level in this system. An earlier report[43] of a band gap of 2.54 eV for Crq_3 in films corresponds to the $\pi \rightarrow \pi^*$ transition from the HOMO−1 level localized on one of the quinolate rings to the LUMO.

The solid-state diffuse reflectance spectrum for the complex (Fig. 12) presents similar bands to those observed in solution, albeit with a small blue shift. The lowest energy band may be slightly shifted from 558 to 543 nm. The diffuse reflectance UV-Visible spectrum of the starting chromium(III) salt, $Cr(NO_3)_3 \cdot 6H_2O$, was also run for comparison. There is a blue shift in the $^4A_2 \rightarrow {}^4T_2$ transition of 34 nm (about 1085 cm^{-1}) on going from the hydrated chromium nitrate salt to Crq_3, indicating a stronger ligand field due to the 8-hydroxyquinolate in the latter case.

Attempts were made to obtain the emission spectrum of this complex in both the solution and the solid state. Upon excitation at 430 nm, a very weak emission was observed

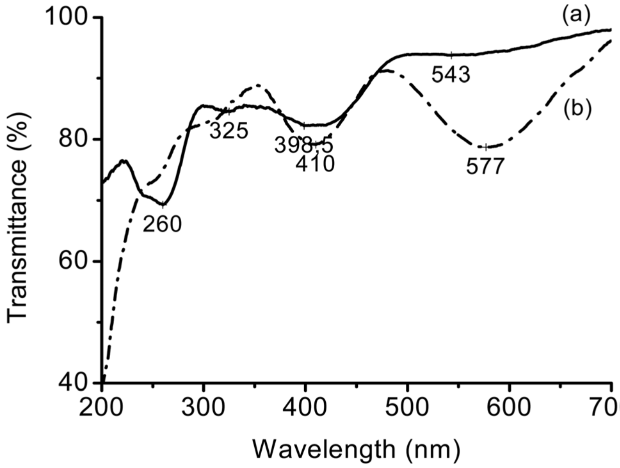

Fig. 12 Diffuse reflectance UV/Visible spectra of (a) Crq$_3$ and (b) Cr(NO$_3$)$_3$·6H$_2$O, in pressed BaSO$_4$ disks.

around 670 nm (quantum yield ≤0.008). The spectrum is given in the ESI.† The behaviour contrasts with the intense green, ligand-based emission in Alq$_3$ ($\lambda_{\text{emission}}$ 535 nm, quantum yield 0.116 in dimethylformamide),[13,78] and related compounds of Al(III),[47,79] Ga(III)[48] and Zn(II),[4] again supporting differences in the natures of the lowest energy excited states. With the compound formed between 8-hydroxyquinoline-5-sulfonate and vanadium(V) oxo ion, the ligand based green emission is weaker than with the free ligand. This is suggested to be due to the presence of low-lying ligand-to-metal charge-transfer state(s).[80] However, the weakness of the emission with Crq$_3$ is attributed to it involving a metal based transition. Further studies are in progress to fully characterize this at room temperature and low temperature.

4. Conclusions

In summary, we have synthesized a *mer*-tris(8-hydroxyquinolinato)-chromium(III) complex, and have fully characterized it by elemental analysis, mass spectrometry, thermogravimetry, FTIR, ^{1}H NMR spectroscopy, X-ray powder diffraction and DFT calculations. The compound forms as a methanol solvate. However, methanol can be removed by heating. Cyclic voltammetry, DFT calculations and UV/Visible absorption and diffuse reflectance spectra allow determination of HOMO and LUMO energies, and are fully consistent with the HOMO being localized on the metal atom. The significantly higher and constant oxidation currents recorded for Crq$_3$ upon repeated cycling, compared with the commonly used Alq$_3$, suggest the potential of this system as an electron transport/hole blocking layer in optoelectronic devices. Future experiments are planned to test this.

Acknowledgements

We are grateful to Professor M. E. S. Eusébio for providing access to the FTIR facilities. The authors thank the financial support of the "The Coimbra Chemistry Centre" from the Fundação para a Ciência e a Tecnologia (FCT), the Portuguese Agency for Scientific Research, through the project PEst-OE/QUI/UI0313/2014 and the Rede Nacional de RMN (REDE/1517/RMN/2005), the Portuguese NMR Network, for spectrometer facilities.

NMR data were collected at the UC-NMR facility which is supported in part by FEDER – European Regional Development Fund through the COMPETE Programme (Operational Programme for Competitiveness) and by National Funds through FCT – Fundação para a Ciência e a Tecnologia (Portuguese Foundation for Science and Technology) through grants REEQ/481/QUI/2006, RECI/QEQ-QFI/0168/2012, CENTRO-07-CT62-FEDER-002012, and Rede Nacional de Ressonância Magnética Nuclear (RNRMN). M. S., L. L. G. J., S. M. F. and M. M. B. also thank the FCT for the postdoctoral grants SFRH/BPD/34372/2007, SFRH/BPD/97026/2013, SFRH/BPD/34703/2007 and SFRH/BPD/72656/2010. In addition, we thank the Laboratory for Advanced Computing at University of Coimbra for providing computing resources that have contributed to the research results reported within this paper (URL http://www.lca.uc.pt).

References

1 J. J. Fox, *J. Chem. Soc.*, 1910, **97**, 1119–1125.
2 K. Soroka, R. S. Vithanage, D. A. Philips, B. Walker and P. K. Dasgupta, *Anal. Chem.*, 1987, **59**, 629–636.
3 M. Roysen, A. Durandin, V. G. Young Jr., N. E. Geacintov and J. W. Canary, *J. Am. Chem. Soc.*, 2006, **128**, 3854–3855.
4 M. L. Ramos, L. L. G. Justino, A. Branco, C. M. G. Duarte, P. E. Abreu, S. M. Fonseca and H. D. Burrows, *Dalton Trans.*, 2011, **40**, 11732–11741.
5 M. A. Palacios, Z. Wang, V. A. Montes, G. V. Zyranov and P. Anzenbacher Jr., *J. Am. Chem. Soc.*, 2008, **130**, 10307–10314.
6 J. P. Phillips, *Chem. Rev.*, 1956, **56**, 271–297.
7 G. H. Jeffery, J. Bassett, J. Mendham and R. C. Denney, *Vogel's Textbook of Quantitative Chemical Analysis*, Longman, Harlow, UK, 5th edn, 1989, pp. 441–442.
8 V. Ravindran, M. R. Stevens, B. N. Badriyha and M. Pirbazari, *AIChE J.*, 1999, **45**, 1135–1146.
9 M. J. Hannon, *Pure Appl. Chem.*, 2007, **79**, 2243–2261.
10 A. R. Timerbaev, *Metallomics*, 2009, **1**, 193–198.
11 G. Bandoli, A. Dolmella, F. Tisato, M. Porchia and F. Refosco, *Coord. Chem. Rev.*, 2009, **253**, 56–77.
12 M. Albrecht, M. Fiege and O. Osetska, *Coord. Chem. Rev.*, 2008, **252**, 812–824.
13 C. W. Tang and S. A. Van Slyke, *Appl. Phys. Lett.*, 1987, **51**, 913–915.
14 K. T. Kamtekar, A. P. Monkman and M. R. Bryce, *Adv. Mater.*, 2010, **22**, 572–582.
15 S. Aihara, Y. Hirano, T. Tajima, K. Tanioka, M. Abe, N. Saito, N. Kamata and D. Terunuma, *Appl. Phys. Lett.*, 2003, **82**, 511–513.

16 J. D. Anderson, E. M. McDonald, M. L. Anderson, E. L. Ritchie, H. K. Hall, T. Hopkins, E. A. Mash, J. Wang, A. Padias, S. Thayumanavan, S. Barlow, S. R. Marder, G. E. Jabbour, S. Shaheen, B. Kippelen, N. Peyghambarian, R. M. Wightman and N. R. Armstrong, *J. Am. Chem. Soc.*, 1998, **120**, 9646–9655.

17 J. L. Bredas, R. Silbey, D. S. Boudreux and R. R. Chance, *J. Am. Chem. Soc.*, 1983, **105**, 6555–6559.

18 A. P. Kulkarni, C. J. Tonzola, A. Babel and S. A. Jenekhe, *Chem. Mater.*, 2004, **16**, 4556–4573.

19 P. E. Burrows, Z. Shen, V. Bulovic, D. M. McCarty, S. R. Forrest, J. A. Cronin and M. E. Thompson, *J. Appl. Phys.*, 1996, **79**, 7991–8006.

20 S. Scholz, C. Corten, K. Walzer, D. Kuckling and K. Leo, *Org. Electron.*, 2007, **8**, 709–717.

21 S. Schmidbauer, A. Hohenleutner and B. König, *Adv. Mater.*, 2013, **25**, 2114–2129.

22 S. Scholz, B. Lüssem and K. Leo, *Appl. Phys. Lett.*, 2009, **95**, 183309.

23 H. D. Burrows, D. Costa, M. L. Ramos, M. da G. Miguel, M. H. Teixeira, A. A. C. C. Pais, A. J. M. Valente, M. Bastos and G. Bai, *Phys. Chem. Chem. Phys.*, 2012, **14**, 7950–7953.

24 F. A. Cotton and G. Wilkinson, *Advanced Inorganic Chemistry*, 5th edn, Wiley, New York, 1988, pp. 679–680.

25 L. Helm and L. A. E. Merbach, *Chem. Rev.*, 2005, **105**, 1923–1959.

26 R. F. P. Pereira, M. J. Tapia, A. J. M. Valente and H. D. Burrows, *Langmuir*, 2012, **28**, 168–177.

27 K. DeArmond and L. E. Forster, *Spectrochim. Acta*, 1963, **19**, 1393–1401.

28 K. DeArmond and L. E. Forster, *Spectrochim. Acta*, 1963, **19**, 1403–1406.

29 A. D. Kirk and G. B. Porter, *J. Phys. Chem.*, 1980, **84**, 887–891.

30 L. E. Forster, *Coord. Chem. Rev.*, 2004, **248**, 261–272.

31 P. S. Wagenknecht and P. C. Ford, *Coord. Chem. Rev.*, 2011, **255**, 591–616.

32 M. Schnuriger, E. Tague and M. M. Richter, *Inorg. Chim. Acta*, 2011, **379**, 158–162.

33 R. B. Lauffer, *Chem. Rev.*, 1987, **87**, 901–927.

34 S. Aime, C. Cabella, S. Collumbatto, S. G. Crich, E. Gianolio and F. Maggioni, *J. Magn. Reson. Imaging*, 2002, **16**, 394–406.

35 E. Taylor-Austin, *Analyst*, 1938, **63**, 710–712.

36 F. Umland and K. Adam, *Z. Anorg. Chem.*, 1965, **341**, 308–323.

37 K. Nakamoto and N. Ohkahu, *Inorg. Chem.*, 1971, **10**, 798–805.

38 J. R. Rao and M. N. Sastri, *Fresenius' J. Anal. Chem.*, 1972, **259**, 286–288.

39 V. Gemmer-Čolos and R. Neeb, *Fresenius' J. Anal. Chem.*, 1980, **97**, 97–100.

40 E. K. Paleologos, C. D. Stalikas, S. M. Tzouwara and M. J. Karayannis, *Anal. Chim. Acta*, 2001, **436**, 49–57.

41 W. G. Hanna and M. M. Moawad, *J. Coord. Chem.*, 2002, **55**, 43–60.

42 M. S. Aksoy, *Asian J. Chem.*, 2009, **21**, 5189–5198.

43 L. M. A. Monzon, F. Burke and J. M. D. Coey, *J. Phys. Chem. C*, 2011, **115**, 9182–9192.

44 X. Xie, X. J. Xiang, J. Liu, X. Y. Ren, H. M. Wang and X. M. Liu, *Inorg. Chim. Acta*, 2012, **383**, 132–136.

45 B. Li, J. Zhang, X. Zhang, J. Tian and G. Huang, *Inorg. Chim. Acta*, 2011, **366**, 241–246.

46 K. Folting, M. M. Cox, J. W. Moore and L. L. Merritt, *Chem. Commun.*, 1968, 1170–1171.

47 M. L. Ramos, L. L. G. Justino, A. I. N. Salvador, A. R. E. de Sousa, P. E. Abreu, S. M. Fonseca and H. D. Burrows, *Dalton Trans.*, 2012, **41**, 12478–12489.

48 M. L. Ramos, A. R. E. de Sousa, L. L. G. Justino, S. M. Fonseca, C. F. G. C. Geraldes and H. D. Burrows, *Dalton Trans.*, 2013, **40**, 3682–3694.

49 A. R. Freitas, *Undergraduate Research Project Report*,University of Coimbra, 2012.

50 M. Kitano, K. Yamagata and Y. Yamazaki, *J. Chem. Soc. Jpn., Pure Chem. Sect.*, 1969, **90**, 190, cited in ref. 38.

51 H. D. Burrows, M. Fernandes, J. Seixas de Melo, A. P. Monkman and S. Navaratnam, *J. Am. Chem. Soc.*, 2003, **125**, 15310–15311.

52 M. W. Schmidt, K. K. Baldridge, J. A. Boatz, S. T. Elbert, M. S. Gordon, J. H. Jensen, S. Koseki, N. Matsunaga, K. A. Nguyen, S. J. Su, T. L. Windus, M. Dupuis and J. A. Montgomery, *J. Comput. Chem.*, 1993, **14**, 1347–1363.

53 A. D. Becke, *J. Chem. Phys.*, 1993, **98**, 5648–5652.

54 C. Lee, W. Yang and R. G. Parr, *Phys. Rev. B: Condens. Matter*, 1988, **37**, 785–789.

55 M. Dolg, H. Stoll, H. Preuss and R. M. Pitzer, *J. Phys. Chem.*, 1993, **97**, 5852–5859.

56 S. Miertus, E. Scrocco and J. Tomasi, *Chem. Phys.*, 1981, **55**, 117–129.

57 J. Tomasi, B. Mennucci and R. Cammi, *Chem. Rev.*, 2005, **105**, 2999–3093.

58 P. E. Schwenn, P. L. Burn and B. J. Powell, *Org. Electron.*, 2011, **12**, 394–403.

59 G. Audi and A. H. Wapstra, *Nucl. Phys. A*, 1993, **565**, 1–65.

60 S. S. S. Raj, I. A. Razak, H.-k. Fun, P.-S. Zhao, F. Jiang, X. Yang, L. Lu and X. Wang, *Acta Crystallogr., Sect. C: Cryst. Struct. Commun.*, 2000, **56**, e130–e131.

61 C. Engekter, H. E. Jackson, C. L. Knight and D. A. Thornton, *J. Mol. Struct.*, 1989, **213**, 133–144.

62 D. A. Thornton, *Vib. Spectrosc.*, 1993, **4**, 309–319.

63 R. Marchon, L. Bokobza and G. Cote, *Spectrochim. Acta, Part A*, 1986, **42**, 537–542.

64 A. D. Esposti, M. Brinkman and G. Ruani, *J. Chem. Phys.*, 2002, **116**, 798–813.

65 C. C. Wagner, A. C. González-Baró and E. J. Baran, *Spectrochim. Acta, Part A*, 2011, **78**, 1762–1765.

66 E. K. Plyler, *J. Res. Natl. Bur. Stand.*, 1952, **48**, 281–286.

67 J. Kidrič, D. Hadži, D. Krocjan and V. Rutar, *Org. Magn. Reson.*, 1981, **15**, 280–284.

68 D. R. Eaton, *J. Am. Chem. Soc.*, 1965, **87**, 3097–3102.

69 B. Pritchard and J. Autschbach, *Inorg. Chem.*, 2012, **51**, 8340–8351.

70 D.-X. Li, D.-J. Xu and Y.-Z. Xu, *Acta Crystallogr., Sect. E: Struct. Rep. Online*, 2003, **59**, m271–m272.

71 A. L. Spek, *J. Appl. Crystallogr.*, 2003, **36**, 7–13.

72 F. Jensen, *Introduction to Computational Chemistry*, Wiley, England, 2nd edn, 2007, ch. 3, p. 93.

73 M. C. Stević, L. M. Ignjatović, G. Ćirić-Marjanović, S. M. Stanišić, D. M. Stanković and J. Zima, *Int. J. Electrochem. Sci.*, 2011, **6**, 2509–2525.

74 F. Papadimitrakopoulos, X.-M. Zhang, D. L. Thompson and K. A. Higginson, *Chem. Mater.*, 1996, **8**, 1363–1365.

75 P. I. Djurovich, E. I. Mayo, S. R. Forrest and M. E. Thompson, *Org. Electron.*, 2009, **10**, 515–529.

76 V. V. N. Ravi Kishore, A. Aziz, K. L. Narasimhan, N. Periasamy, P. S. Meenakshi and S. Wategaonkar, *Synth. Met.*, 2002, **126**, 199–205.

77 B. Bosnich, *J. Am. Chem. Soc.*, 1968, **90**, 627–632.

78 F. E. Lytle, D. R. Storey and M. E. Juricich, *Spectrochim. Acta, Part A*, 1973, **29**, 1357–1369.

79 C. H. Chen and J. Shi, *Coord. Chem. Rev.*, 1998, **171**, 161–174.

80 M. L. Ramos, L. L. G. Justino, S. M. Fonseca and H. D. Burrows, *New J. Chem.*, 2015, **39**, 1488–1497.

Electronic supplementary information (ESI)

Synthesis, structure, spectral and electrochemical properties of chromium(III) *tris*-(8-hydroxyquinolinate)

Ana R. Freitas, Mónica Silva, M. Luísa Ramos, Licínia L. G. Justino, Sofia M. Fonseca, Madalina M. Barsan, Christopher M. A. Brett, M. Ramos Silva, Hugh D. Burrows*

Assignment of bands in FTIR spectra

Table S1. FT-IR spectral data obtained using ATR for Crq$_3$ solid

Band/cm^{-1}	Tentative assignment[a]
525	In-plane ring deformation
572	In-plane ring deformation
635	Out-of-plane ring deformation
743	Out-of-plane C-H bend
781	Out-of-plane C-H bend
822	Out-of-plane C-H bend
873	In-plane C-H bend
1053	In-plane ring deformation
1107	In-plane C-H bend, C-O stretch
1166	In-plane C-H bend
1216	Ring stretching; In-plane C-H bend
1274	In plane C-H bend
1316	Ring stretching
1371	Ring stretching
1459[b]	C-O stretch
1492	Ring stretching
1571	C=C stretch
1595	C=N stretch
2866[b]	C-H stretch
2960[b]	
2964[b]	
3053	
3325	O-H stretch

a. Using assignments from references 1 and 2.

b. Bands attributed to methanol from spectral data in reference 3.

Use of Crq_3 as an NMR Relaxation Agent

The Cr(III) metal complex can act through pseudocontact interactions as a good relaxation agent of non-complexed molecules in solution, as shown in Figures S1 and S2. Here the ^1H NMR signals of unbound 8-Hq molecules (outer-sphere) are observed to be increasingly broadened with the addition of the Crq_3 complex with no significant change in the chemical shifts.

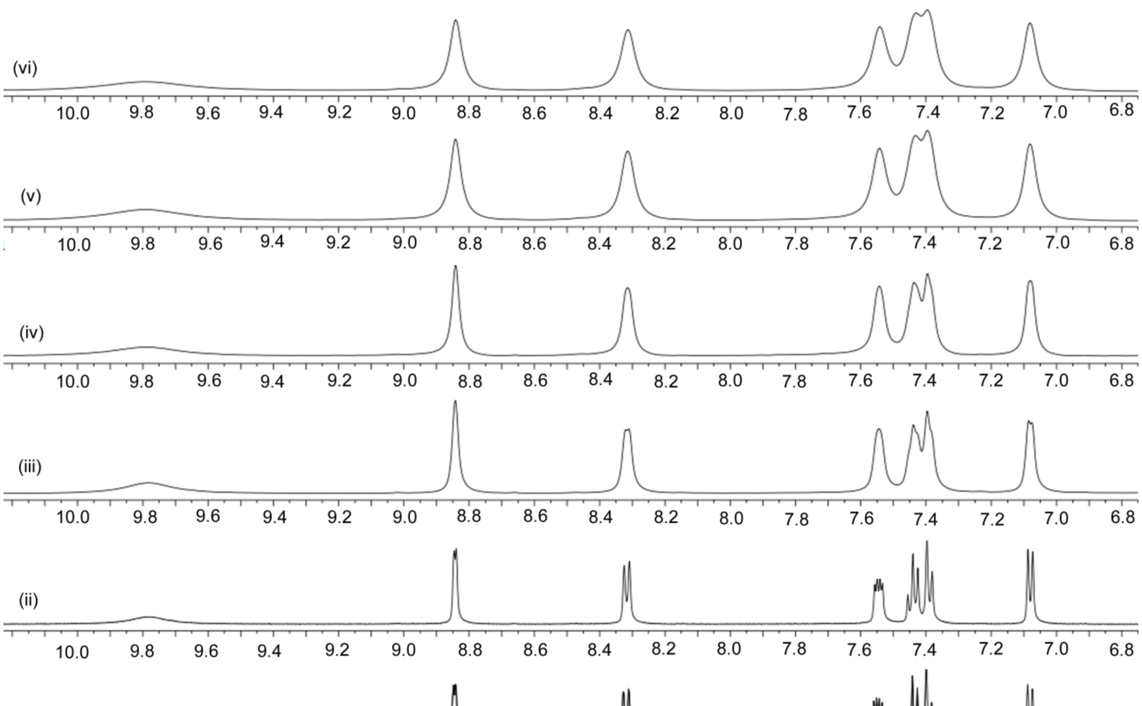

Fig. S1. Expansions from 6 to 11 ppm (8-Hq signals) of ^1H NMR spectra (499.824 MHz) of DMSO-d_6 solutions of (i) 8-Hq 10 mmol dm^{-3}, (ii) Crq_3:8-Hq 2:10 mmol dm^{-3}, (iii) Crq_3:8-Hq 4:10 mmol dm^{-3}, (iv) Crq_3:8-Hq 6:10 mmol dm^{-3}, (v) Crq_3:8-Hq 8:10 mmol dm^{-3}, and (vi) Crq_3:8-Hq 10:10 mmol dm^{-3}, 298 K.

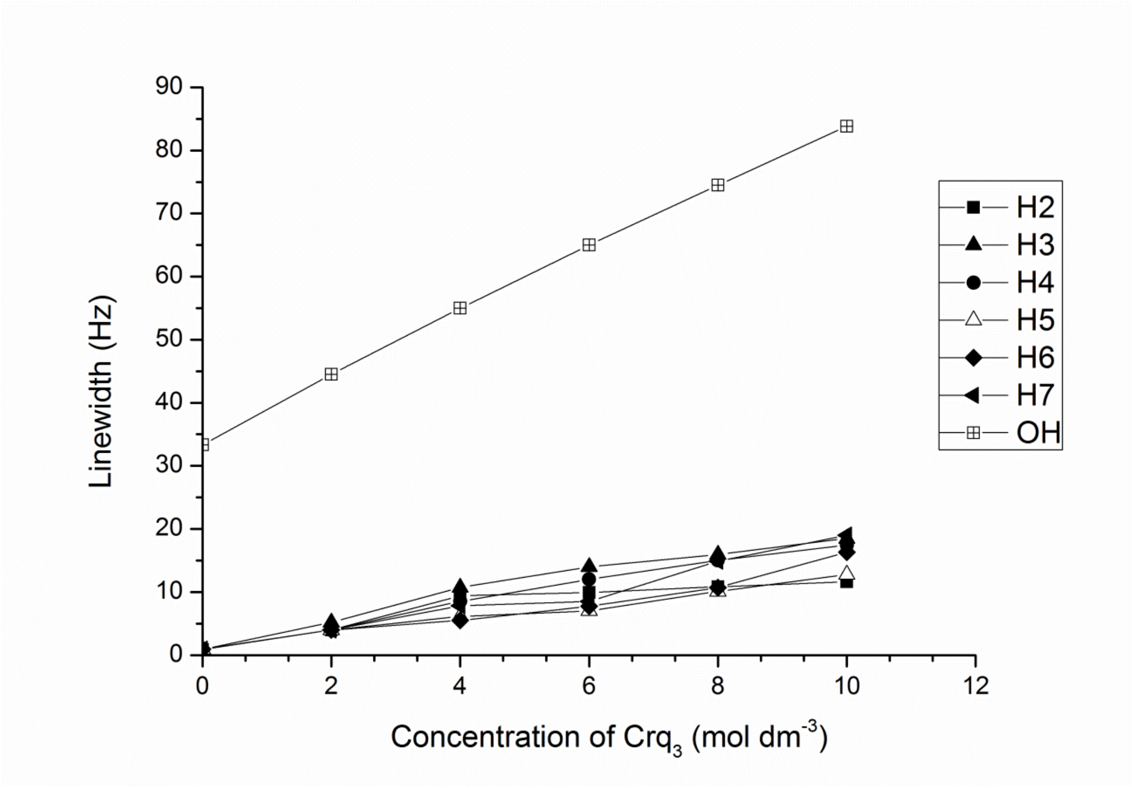

Fig. S2. Line width (Hz) of the ^{1}H NMR signals of 8-Hq 10 mmol dm^{-3}, in DMSO-d_6 solution, as a function of the concentration of Crq$_3$ added to the solution.

Photoluminescence spectrum

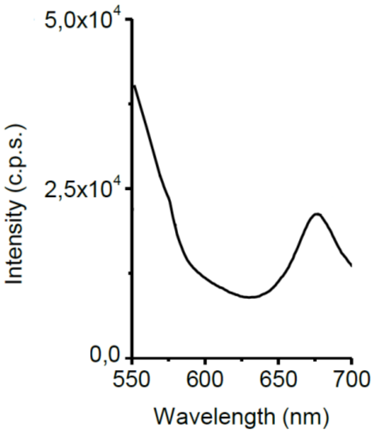

Fig. S3. Luminescence spectrum of Crq$_3$ in DMSO solution at room temperature ($\lambda_{excitation}$ 430 nm). The apparent emission below 550 nm is due to a Raman band.

References

1. R. Marchon, L. Bokobza, G. Cote, *Spectrochim. Acta A* 1986, **42A**, 537-542.
2. C. C. Wagner, A. C. González-Baró, E. J. Baran, *Spectrochim. Acta Part A*, 2011, **78**, 1762-1765.
3. E. K. Plyler *J. Res. Natl. Bureau Standards* 1952, **48**, 281- 286